NANO · MICRO small
www.small-journal.com

pH Tunable Patterning of Quantum Dots

Ilker Torun, Conan Huang, Mustafa Kalay, Moonsub Shim, and M. Serdar Onses**

Patterning of quantum dots (QDs) is essential for many, especially high-tech, applications. Here, pH tunable assembly of QDs over functional patterns prepared by electrohydrodynamic jet printing of poly(2-vinylpyridine) is presented. The selective adsorption of QDs from water dispersions is mediated by the electrostatic interaction between the ligand composed of 3-mercaptopropionic acid and patterned poly(2-vinylpyridine). The pH of the dispersion provides tunability at two levels. First, the adsorption density of QDs and fluorescence from the patterns can be modulated for pH > ≈4. Second, patterned features show unique type of disintegration resulting in randomly positioned features within areas defined by the printing for pH ≤ ≈4. The first capability is useful for deterministic patterning of QDs, whereas the second one enables hierarchically structured encoding of information by generating stochastic features of QDs within areas defined by the printing. This second capability is exploited for generating addressable security labels based on unclonable features. Through image analysis and feature matching algorithms, it is demonstrated that such patterns are unclonable in nature and provide a suitable platform for anti-counterfeiting applications. Collectively, the presented approach not only enables effective patterning of QDs, but also establishes key guidelines for addressable assembly of colloidal nanomaterials.

1. Introduction

Colloidal quantum dots (QDs) have attracted significant interest for applications in light emitting diodes,[1] displays,[2] solid-state lighting,[3] sensing,[4] solar cells,[5] optogenetics,[6] and anti-counterfeiting.[7] The strong interest in these nanoscale materials emerge from the size-dependent luminescence properties.[8] The progress in chemical synthesis approaches has allowed for colloidal QDs with very low levels of polydispersity, resulting in solution-processable nanoscale materials with narrow spectral emission bandwidths and high quantum yields.[9–11] However, the majority of high-technology applications require precise patterning and assembly of QDs over solid surfaces and films. In display applications, for example, there is a need for the definition of individual red, green, and blue (RGB) pixels at high integration density.[12] In anti-counterfeiting applications,[13,14] patterning of QDs with different luminescence properties on the same substrate is an efficient approach for increasing the entropy and therefore exponentially increasing the difficulty of pattern duplication. Hierarchical patterning of QDs can also be useful in encoding applications. The formation of random domains of QDs within the patterned regions is an effective way to fabricate unclonable surfaces.[15] ernin Approaches are needed for multiplexed patterning of QDs with precise control over the size and geometry. Such approaches should also enable expanding the entropy through generation of random features composed of QDs of high purity colors.

To date, significant progress has been made in the patterning of QDs. Colloidal QDs can be deposited using different techniques such as electrospraying,[16] spin-coating,[17] Langmuir–Blodgett,[18] and dip-coating[19] yielding homogeneous films. Although these approaches have excellent thickness fidelity, control over spatial position is missing. One approach to pattern QDs is to combine these deposition techniques with templates

I. Torun, M. S. Onses
Department of Materials Science and Engineering
Nanotechnology Research Center (ERNAM)
Erciyes University
Kayseri 38039, Turkey
E-mail: onses@erciyes.edu.tr

The ORCID identification number(s) for the author(s) of this article can be found under https://doi.org/10.1002/smll.202305237

DOI: 10.1002/smll.202305237

I. Torun, C. Huang, M. Shim
Department of Materials Science and Engineering
University of Illinois Urbana–Champaign
Urbana, IL 61801, USA
E-mail: mshim@illinois.edu

M. Kalay
Nanotechnology Research Center (ERNAM)
Erciyes University
Kayseri 38039, Turkey

M. Kalay
Department of Electricity and Energy
Kayseri University
Kayseri 38039, Turkey

M. S. Onses
UNAM–Institute of Materials Science and Nanotechnology
Bilkent University
Ankara 06800, Turkey

fabricated by various forms of lithography. Conventional manufacturing approaches including electron-beam lithography,[20] nanoimprint lithography,[21] and photolithography[22] have been explored to prepare templates for spatially controlled deposition of QDs. As the essential manufacturing technique used in the semiconductor industry, photolithography has been actively studied for fabricating patterns of QDs. The large area fabrication and ease of adoption in industrial setting are the main advantages of photolithographic techniques.[23] The key challenge is the incompatibility between colloidal QDs and chemicals, e.g., photoresist, solvent, and developer, used in the lithography process. Innovative approaches in ligand engineering can address this issue by directly using colloidal QDs as photoresist layers.[24–26] In addition to delicate chemical processes to prepare such engineered nanoscale emitters, multiplex patterning is challenged by the repeated deposition of QDs over the entire substrate and lithographic development steps. Another widely utilized approach to pattern QDs is transfer printing[27–29] from a donor substrate. Pixelated luminescent features of RGB emitting QDs were effectively fabricated with different form of transfer printing.[30] The need for patterned stamps and/or substrates together with varying degrees of defect tolerance and resolution are critical considerations for certain applications. In a complementary manner, various forms of ink-jet printing show great promise with its simplicity, low-cost, and additive nature. The direct deposition of colloidal QDs in pixelated geometries with multiple photoluminescence (PL) properties over flexible substrates are the key advantages of these techniques. Conventional ink-jet printing[31,32] techniques are effective in defining pixels at a size that approach couple of tens micrometers. This resolution can be further improved by using advanced forms of printing techniques such as electrohydrodynamic jet (e-jet) printing,[33] bubble printing,[34] and dip-pen nanolithography.[35] Each of these patterning techniques from photolithography to ink-jet printing have their own set of merits. Advanced technological applications will greatly benefit from assembly approaches that are adaptable to these patterning techniques and enable tunable organization of multiple colloidal QDs over functional patterns with microscopic and nanoscopic dimensions.

In this study, we present pH tunable assembly of QDs through selective adsorption over patterns of polymers. Aqueous dispersions of QDs with precisely defined pH is prepared by colloidal synthesis followed by ligand exchange and pH adjustment processes. Patterns of poly(2-vinylpyridine) (P2VP) are prepared by e-jet printing.[36] The choice of P2VP[37,38] stems from the ability of selective adsorption of colloidal nanomaterials through electrostatic interactions as demonstrated with spherical[39] and rod-shaped[40] gold nanoparticles, and nanoplatelets.[41] An additional characteristic of this polymer is the protonation and deprotonation of the pyridine group allowing for pH tunable assembly of QDs. The pH of the dispersion is exploited for the tunable assembly QDs in two routes: (i) The adsorption density of QDs and fluorescence from the patterns can be tuned with the pH, (ii) randomized QD domains emerge from the patterned region for pH $\leq \approx 4$. This tunability is particularly appealing for encoding applications. The uniform patterns prepared at pH 5, for example, are useful for deterministic encoding of information. The second route enables hierarchically structured encoding by generating stochastic features of QDs within areas defined by the printing. We particularly focus on the second route and demonstrate unclonable features of QDs within different geometric forms. The authentication of the unclonable features is successfully performed by using binary keys and feature matching algorithms. The adaptability of the presented pH tunable assembly approach to fabrication techniques other than printing enhances the application potential.

2. Results and Discussion

Figure 1 presents schematics and key results regarding pH tunable patterning of QDs. The first step consists of e-jet printing of P2VP to generate functional binding sites. E-jet printing directly defines patterns of P2VP in an additive manner without any contamination or residual layer. An important advantage of using solutions of polymers rather than colloidal dispersions as inks is improving printability and minimization of clogging issues.[42,43] On top of the P2VP patterns, QDs are deposited by drop-casting. The selective assembly of QDs over patterns of P2VP is achieved by electrostatic interactions.[37,40] The excess and unadsorbed QDs are then removed by rinsing in water. The selective adsorption on the P2VP requires the QDs to be in aqueous phase[44] (Figure 1b). For this purpose, QDs prepared in the organic solvents were processed to enable dispersion in water. Immediately prior to selective adsorption, pH of the QD solution was adjusted by addition of hydrochloric acid or sodium hydroxide. The immobilization of water-dispersed QDs results in high density and selective assembly over the patterns of P2VP defined by e-jet printing (Figure 1c). The adsorption of QDs onto the P2VP patterns strongly depended on the pH of the QD dispersion (Figure 1d). The highest adsorption density was achieved at pH 5 and the density of assembled QDs decreased as the pH of the dispersion become distant from this value. At very low pH values, the disintegration of P2VP patterns provides intriguing ways to prepare stochastic features for encoding applications.

The versatility of e-jet printing in patterning of P2VP is demonstrated by fabricating features of varying size and geometry. To this end, arrays of dots over large areas (Figure 1e) can be printed by continuous application of voltage pulses in e-jet printing. In addition to dots, linear features (Figure 1f) can be fabricated by tuning the jetting parameters and stage translation speed. Figure 1g presents 3D profile of printed features obtained by AFM imaging. There is a certain degree of variation in the height ($41.3\ \text{nm} \pm 4.9\ \text{nm}$) of the features inherent to the printing of concentrated polymer solutions from solvents of low volatility. SEM imaging (Figure 1h) of an array of P2VP features shows that the average size of features was 1.1 μm with a standard deviation of ≈0.1 μm. The electric field assisted jetting process allows for generating patterns with feature sizes that range from microscopic to nanoscopic dimensions (Figure 1h–i; Figure S1 (Supporting Information) for additional SEM and optical microscope images). Previous work has shown the feasibility of achieving sub-100 nm features with e-jet printing.[45] SEM imaging confirms complete coverage of the P2VP features with QDs following the assembly and washing process (Figure S2, Supporting Information). On-demand printing of complex geometries[46] such as the bird shown in Figure 1c demonstrates the advanced level of control in the patterning process (see Figure S3 in the Supporting Information for different pattern geometries). Multiplex patterning of

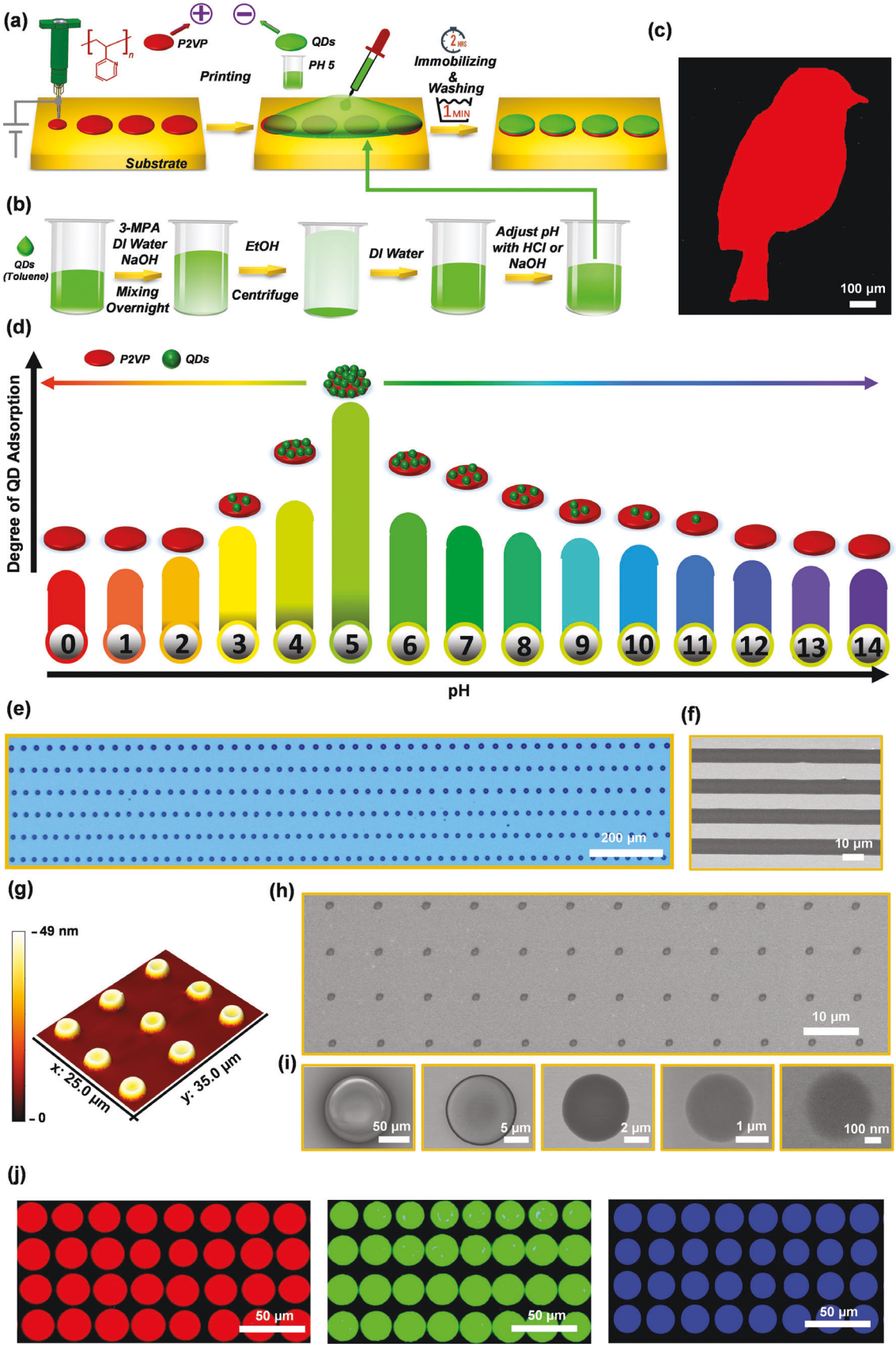

QDs is possible by sequential printing and assembly processes (Figure S4a, Supporting Information). The presented approach is adaptable to flexible PDMS and transparent glass substrates (Figure S4b, Supporting Information). The approach can be readily extended to QD emitters of different sizes that emit light in the essential pixelation colors of RGB (Figure 1j). These results confirm homogeneous assembly of QDs over patterns of P2VP.

We first studied the e-jet printing of P2VP to define the binding sites for adsorption of QDs. The printing speed and bias voltage, in particular, were varied and the morphology of the printed polymer features were analyzed using AFM. **Figure 2** summarizes the results. At a fixed bias voltage, linear and dot like features can be obtained by varying the printing speed, which was controlled through the movement speed of the underlying stage. The printing speed inversely relates to the amount of material deposited per unit time in close agreement with previous studies.[46] The increasing speed resulted in the reduction of the height and width of the lines. At stage speeds higher than 400 μm s^{-1}, discontinuous features with spaced dots were obtained. The diameter of the dot remained similar, while the spacing between the dots increased at high (3.2 mm s^{-1}) printing speeds. At a relatively high printing speed of 2 mm s^{-1}, the bias voltage dependence (varied between 450 and 250 V) was also examined. At these conditions, dot like features were obtained. The height and width of the dots increased with increasing the bias voltage. An interesting observation is bowl like features obtained at high voltages. This type of morphology likely relates to the coffee-ring effect,[47] where the material is transported from center to the edge. This type of height variation across the P2VP features becomes larger with the increase of the diameter. This height variation, to a certain extent, affects the immobilization of QDs. Previous research[39] has shown the increased adsorption density of colloidal nanoparticles on nonplanar features in comparison to the flat films.

Aqueous dispersions of the QDs of varying pH were prepared by colloidal synthesis in an organic solvent followed by ligand exchange to transfer to the aqueous phase and pH adjustment. **Figure 3**a presents PL spectra and TEM images of as-purified QDs in toluene. The preparation of the QD inks for immobilization and patterning on the polymer substrates began with the synthesis of bright QDs via a 1-pot colloidal approach modified from previous methods.[48–50] Hot injection of anion precursor into Cd and Zn containing organometallic complexes yielded highly tunable and fluorescent cores, which was then followed by high-temperature shelling with either tri-octylphosphine selenide (TOP-Se), tri-octylphosphine sulfide (TOP-S), or polysulfide precursor such as ODE-S or OA-S. This process yields 72%, 54%, and 82% quantum yield with a full width at half maximum < 30 nm (after purification via acetone and ethanol or acetonitrile) for QDs composed of CdZnSe/ZnSe, CdZnSe/ZnS, and CdZnS/ZnS (see Table S1 in the Supporting Information for details), respectively. To transfer the QDs to a compatible solvent, the nanoparticles were dispersed in water via a modified approach by recapping with a hydrophilic ligand, 3-mercaptopropionic acid (3-MPA). The PL was reduced for blue and red QDs as a result of ligand exchange as seen in Figure 3. This reduction is attributed to hole trapping due to full exchange of anion sites, as thiols are well known in the literature to serve as hole traps,[51] and it especially affects blue color materials. These QD solutions were then adjusted to the proper pH as in **Figure 4**a (see Figure S5 in the Supporting Information for details). The solution pH is critical for controlling the QD immobilization density. In Figure 3c, we observe only a small effect of HCl addition towards a pH of ≈5, leaving stable, bright RGB QDs suitable for the immobilization on P2VP patterns. Additional characterization of QDs in different pH solutions are shown in Figures S6 and S7 in the Supporting Information. The PL decreased with the decreasing pH value, whereas the PL wavelength remained unchanged. The zeta potential values (see Figures S8 and S9 in the Supporting Information for details) of the red and green QDs after ligand exchange and at pH 5 confirmed the highly negative surface charge of the materials.

The selective adsorption of QDs onto the printed patterns of P2VP strongly depended on the pH of the aqueous QD dispersion. Figure 4a presents the schematic illustration and fluorescence microscopy images of the printed arrays of RGB QDs immobilized from dispersion with pH values ranging from 3 to 8. At identical measurement conditions, the fluorescence intensity correlates with the density of QDs immobilized on the patterned features. The fluorescence intensity for all three colors of QDs was highest at a pH of 5, suggesting that the adsorption onto the P2VP patterns was maximized at this pH. Considering the p*Ka* value of pyridine is ≈5.2, the partial protonation of the patterns is expected at a pH of 5.[37,40] QDs are effectively immobilized over the positively charged P2VP patterns at a pH of 5 through electrostatic interactions. The fluorescence intensity decreased with deprotonation of P2VP at higher pH values (e.g., 6–8), supporting the electrostatic interaction mediated assembly of QDs over the patterns. At pH values lower than 5, the fluorescence from the patterns was not uniform. Rather, randomly positioned bright spots within the region defined by the printing was obtained. This result implies a competition between two effects, namely protonation and dissolution of P2VP at low pH values. P2VP becomes water soluble at pH < 5.[52] Therefore, adsorption of QDs from an aqueous solution at these acidic conditions results in disintegration of the P2VP patterns. We hypothesize that the rapid adsorption of QDs at random sites within the patterns protects the underlying P2VP from dissolution resulting in such an assembly. The complete coverage of localized P2VP sites with QDs likely contributes to this observation. AFM images presented in **Figure 5**b further support this hypothesis, as the height

Figure 1. Assembly of QDs on patterns of P2VP prepared by e-jet printing. a) Schematic illustration of the patterning process. The printing is performed by using 10% P2VP in 1,2,4 trichlorobenzene with a metal-coated glass nozzle (1, 2, or 5 μm inside diameter at the tip). QDs of three different colors are assembled over the patterns: CdZnSe/ZnS red, CdZnSeS/ZnS green, and CdZnS/ZnS blue b) Schematic showing the exchange of QDs from the organic phase to the water phase. c) Printing complex geometries. Fluorescence microscope image of red QDs assembled on the e-jet printed P2VP patterns. d) Schematic illustration showing the pH dependent assembly of QDs. The adsorption density of QDs depends on the pH of the QD dispersion in water. e) Optical microscope image of a large-area array of printed P2VP dots. f) SEM image of an array of P2VP lines. g) AFM image of an array of P2VP dots. h) Large-area view SEM image of an array of P2VP dots. i) SEM images of P2VP dots of varying size. j) Fluorescence microscope images of arrays of RGB QDs assembled on the P2VP patterns.

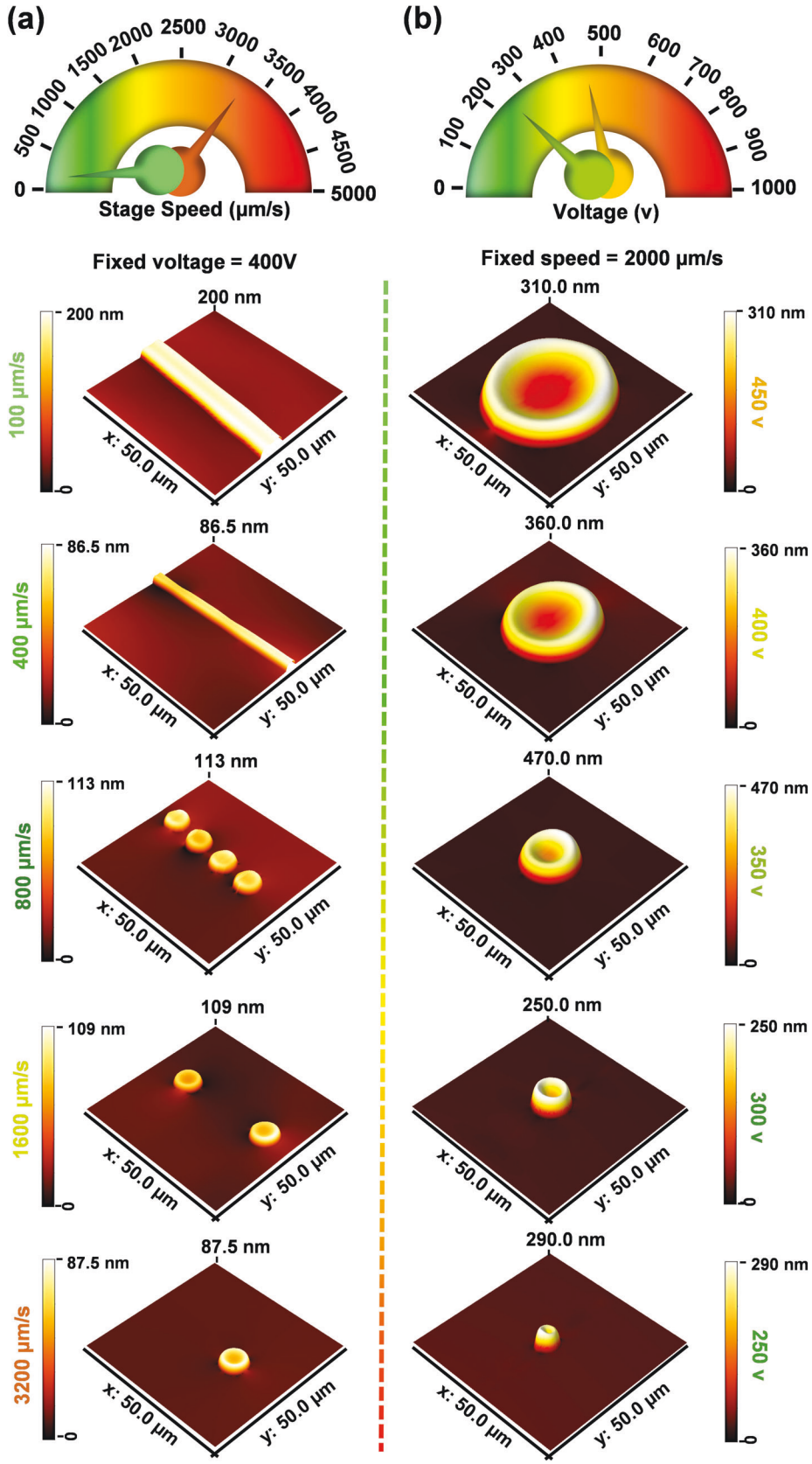

Figure 2. Effects of stage speed and voltage bias on the height profile of e-jet printed P2VP patterns. AFM images for a) varying stage speed at a fixed voltage bias and b) varying voltage bias at a fixed stage speed.

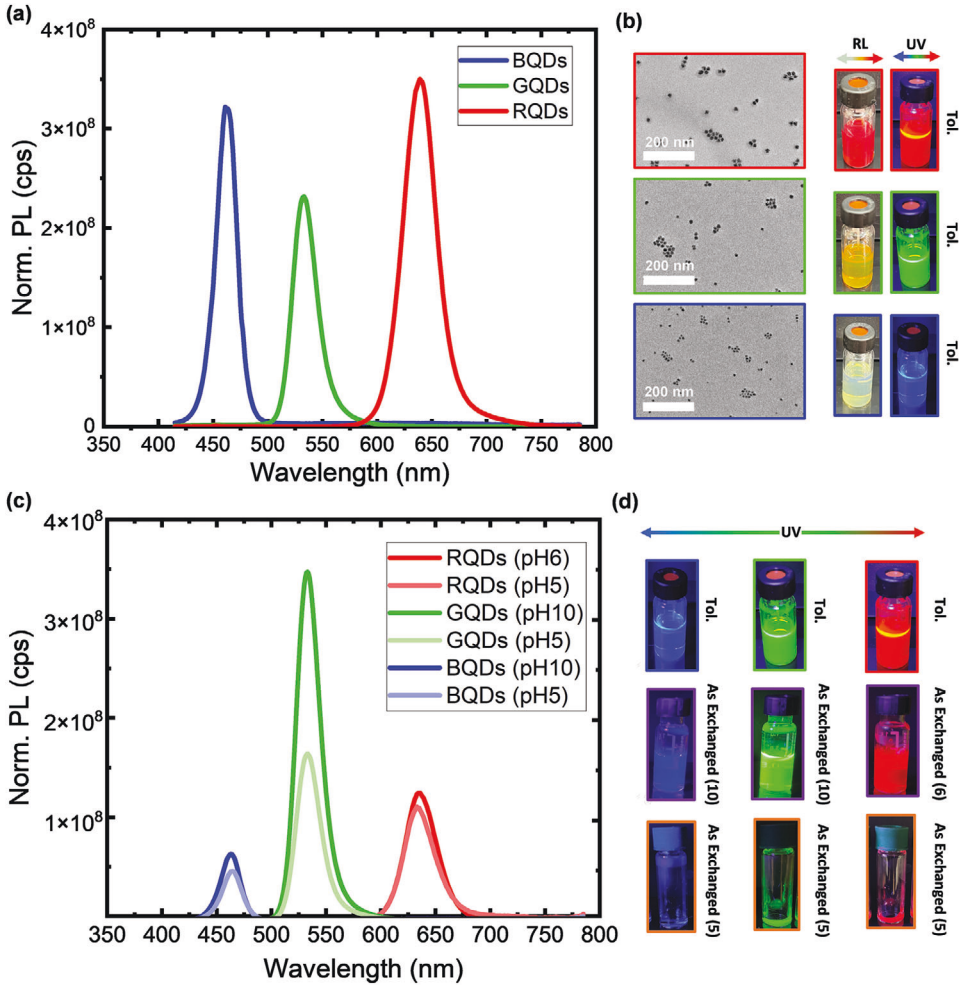

Figure 3. Absorbance normalized PL signals of resulting QDs excited at a) 400 nm in the purified toluene phase, b) TEM showing the resulting materials and their PL properties under room light (RL) and UV light. c) The resulting PL signals (normalized to the absorbance at the excitation wavelength, λ = 400 nm) of QDs as exchanged into the aqueous phase with 3-MPA stabilizing ligand (bottom) and adjusted to pH 5 for immobilization and d) various photoluminescent properties of the QDs with native ligand in toluene, as exchanged in water, and adjusted to pH 5 for immobilization under UV excitation.

of randomly positioned features is close to the height of the initially printed P2VP patterns (see Figure S10 in the Supporting Information for additional AFM images). The extent of fluorescent sites becomes lower at pH of 3 in comparison with pH of 4. The effect of pH of the QD dispersion on the assembly can be clearly seen in the fluorescence microscope images taken at two different exposure times (Figure S11, Supporting Information). At pH 10, the patterns are weakly visible even at an exposure time as high as 30 s, whereas bright fluorescence is observed at pH 5 for an exposure time of 3 s. The fluorescence reaches saturation at high exposure times for QD dispersions with a pH of 5. An additional consideration here is that the conformation of P2VP chains switch from globule to extended coil when the pH is reduced below 4.[53] In cross-linked thin films of P2VP, the exposure to acidic solutions with a pH of 2 resulted in significant folding.[54] This type of folding was prevented when a top-layer of polystyrene was used.[55] Note that P2VP film is not cross-linked in this study. The rapid adsorption of QDs in our system can serve as a protective layer to prevent disintegration of the underlying P2VP films. This type of unique disintegration of P2VP patterns was studied for the generation of unclonable surface features in the following section. The transformation from uniform patterns to random surface features significantly improves the entropy and makes duplication practically very difficult. The pH dependence of the fluorescence was similar for RGB light emitting QDs immobilized onto the P2VP patterns. The fluorescence intensity from the patterns depended on the immobilization time and reached a plateau after ≈2 h of the immobilization (see Figure S12 in the Supporting Information for additional images and schematics). This type of kinetics resembles adsorption of negatively charged colloidal nanomaterial on surfaces modified with end-grafted P2VP layers.[56] The fluorescence from the patterns exhibited high-level of ambient stability. The integrated brightness intensity values remained > 88% at the 180th day of ambient storage (Figure S13, Supporting Information).

Finally, we demonstrate the application of the proposed assembly approach in the preparation of security labels with stochastic

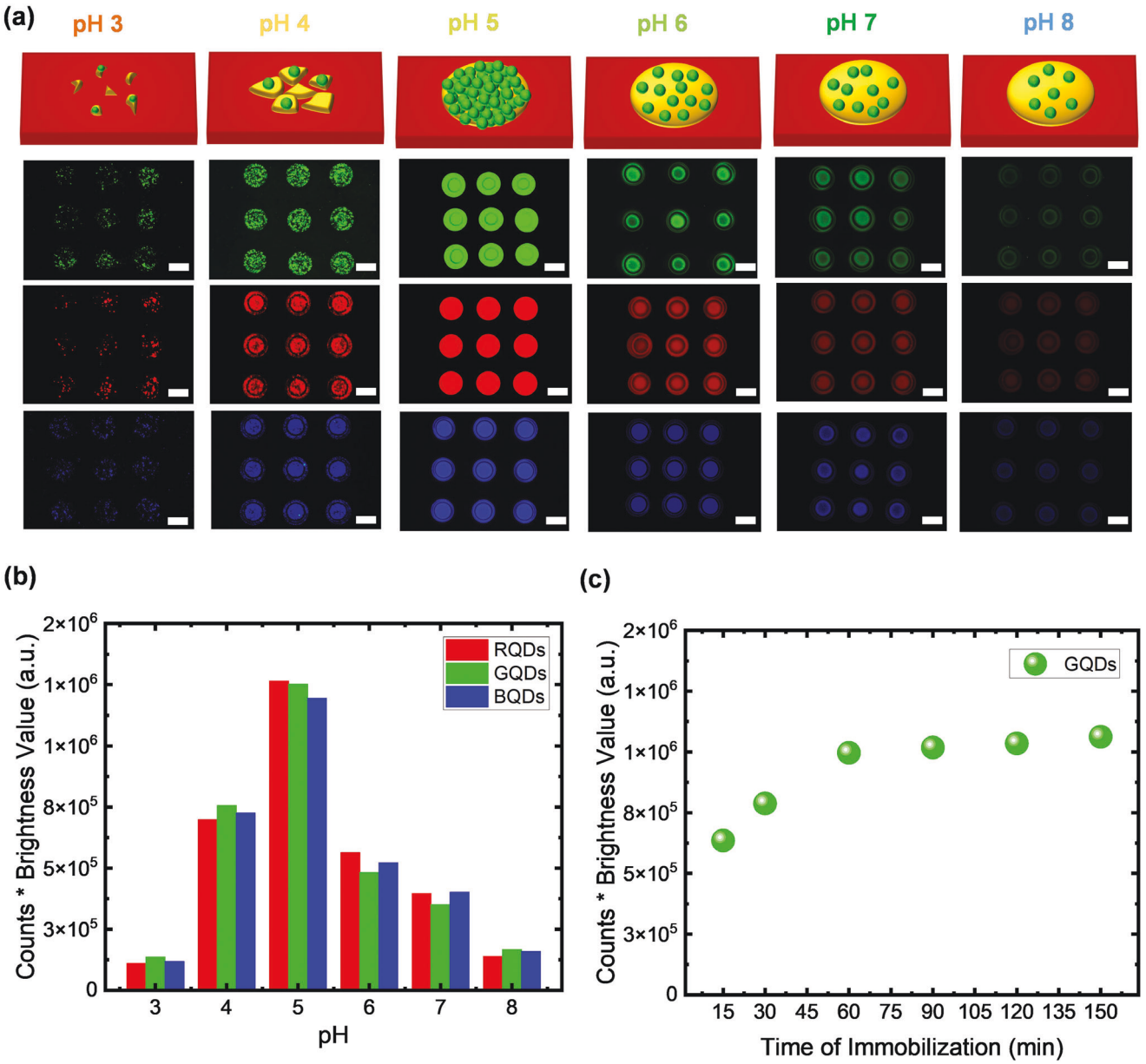

Figure 4. Effect of the immobilization time and pH on the assembly of QDs on the e-jet printed patterns of P2VP. a) Schematic representation and fluorescence microscope images of P2VP dots following assembly of QDs at a pH of 5 for different immobilization durations. All scale bars are 100 µm. The exposure time is 3 s in fluorescence microscope images. b,c) Integrated brightness intensity as a function of the (b) pH and (c) immobilization time. The intensity was analyzed by greyscale conversion and measurement of the pixel value as described in the Experimental Section.

and deterministic components. There is a growing interest in encoded surfaces for applications in anti-counterfeiting and authentication. Luminescent materials have attracted enormous interest as encoding elements, due to their size dependent and distinct luminescence wavelengths, fluorescence lifetime and narrow full-width-at-maximum values, and fluorescence longevity.[57] Patterning QDs in 1D and 2D barcodes, for example, is one approach to prepare security labels.[58,59] However, the broad adoption of these materials together with their increased availability make such security labels vulnerable to counterfeiters and third parties. A promising solution is to exploit stochastic processes to fabricate unclonable surfaces. The concept of physically unclonable functions (PUFs)[60] relies on physical systems in encoding. PUFs produce a unique response to an applied challenge using a stochastic process.[61] The use of PUFs, in principle, makes the replication of the security labels impossible by the encoder and third parties. Chemical processes with inherent stochasticity is receiving growing attention.[62,63] An effective approach[15] is hierarchical patterning of QDs through stochastic arrangement of nanoscale materials within deterministically defined sites prepared by

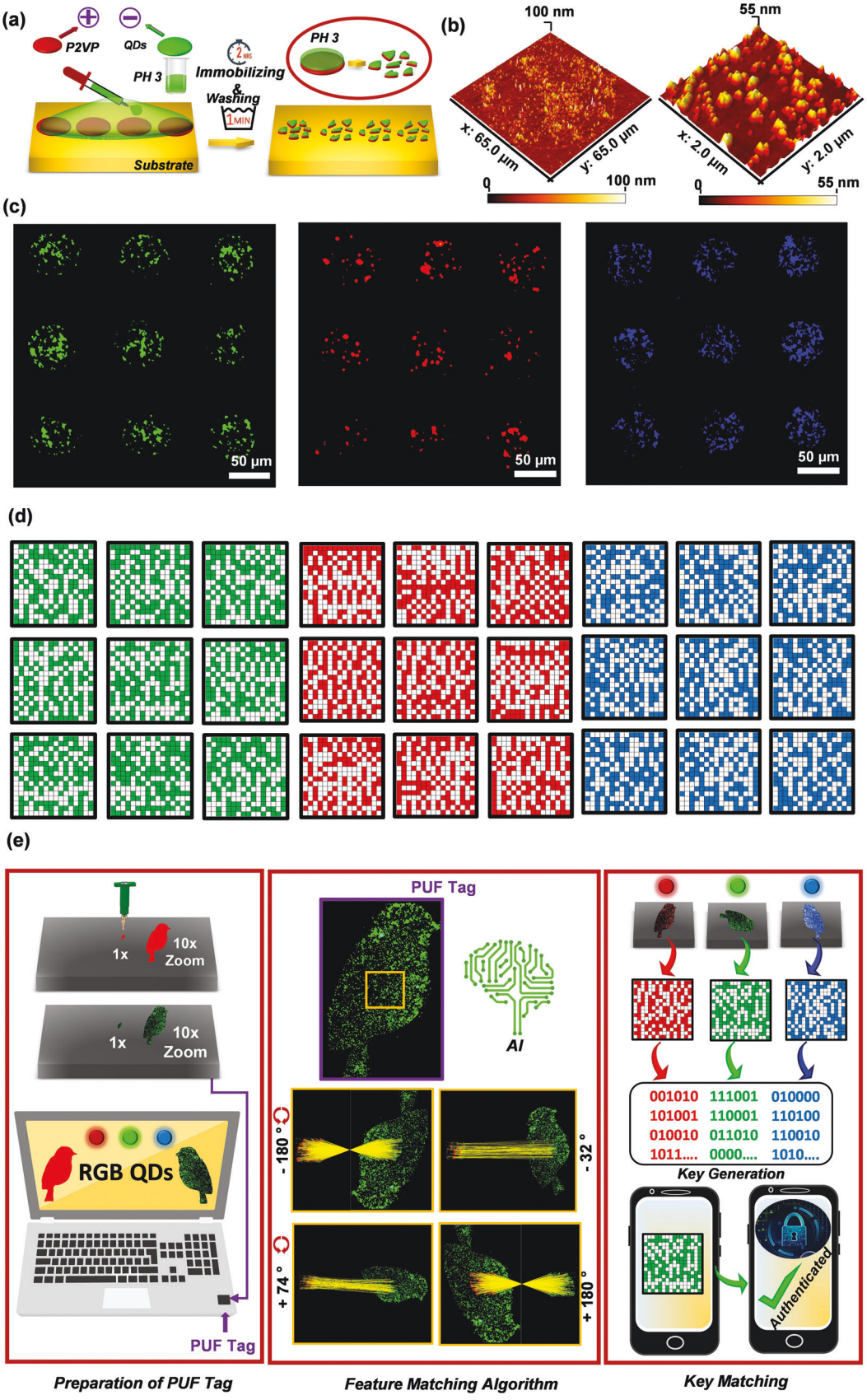

ink-jet printing. Particularly facile and quick approaches, which can be easily mass produced but very difficult to replicate at scale even with state-of-the-art inkjet printing processes are needed.

The tunable nature of the presented assembly approach presents different routes for the preparation of encoded surfaces. The uniform patterns prepared at pH 5, for example, are useful for conventional barcode-like security labels. The randomly positioned fluorescent features formed at low pH values prompts their usage in construction of addressable PUFs. We choose the latter approach in this study. Figure 5 presents the key results and schematic illustration of the concept. An array (3 × 3) of P2VP dots were fabricated by e-jet printing. The immobilization of QDs of three different colors were then performed at pH 3, followed by a washing in water. The disintegration of P2VP features resulted in random features in regions defined by the printing. AFM imaging (Figure 5b) of the features shows that the polymer disintegrates and forms random spots at this pH value rather than random positioning of QDs over the uniform P2VP spots. Figure 5c demonstrates the ability to generate such patterns for green, red, and blue QDs. These patterns can be converted into binary keys (Figure 5d), which are composed of bits mapped to the detection of QD fluorescence. Security keys were generated from green, red, and blue fluorescent images. The keys here were obtained by applying the Von Neumann Debiasing algorithm (see Figure S14 in the Supporting Information for details of the key extraction process). These keys can be stored to a data base and authentication can be performed by comparison of the binary keys. The analysis of binary keys extracted from the fluorescence microscope images enables evaluation of the PUF performance. Figure S15 in the Supporting Information presents the commonly[39] used metrics calculated from the binary keys. These results show that the distribution of 0-bits and 1-bits is close to the ideal value of 0.5 and relative difference between multiple binary keys as measured by the interchip Hamming distance is centered around 0.5. The randomness of the binary keys is further confirmed by p-values being greater than 0.01 (Table S2, Supporting Information).

An advanced and aesthetically favorable approach is to construct a complex image from randomly positioned features. Figure 5e presents an example with a bird. At low magnification, this bird serves as the first layer of security, where the geometry and luminescence wavelength are deterministically defined by the manufacturer. At a high magnification fluorescence microscopy image, randomly positioned features appear. These features can be stored in a data base. In a practical setting, one can challenge the authenticity of the product by taking a fluorescence microscopy image from the bird image. Feature matching algorithms can effectively authenticate even if the fluorescence microscope image is taken only from a part of the bird or the bird is rotated at different angles. Key points in the fluorescence microscope image taken from a part of the bird or rotated at different angles were identified and stored as objects. Figure 5e presents a demonstration using an advanced feature matching algorithm ORB[64] (Oriented FAST and Rotated BRIEF). The main reason for using the ORB algorithm is that it provides faster results in images taken under various magnification conditions and at different rotation angles.[65] As a result of this algorithm, matching features are shown with yellow lines. In practice, such features can be authenticated via comparison of the fluorescence microscope images taken at multiple wavelengths with the database constructed by the manufacturer. The matching of binary keys and features between the image and database ensures authenticity of the product.

3. Conclusion

We have presented an approach for addressable assembly of colloidal QDs on patterns of P2VP prepared by additive jet printing. The key idea is the pH dependent selective adsorption of QDs over a patterned polyelectrolyte with an active pyridine chemical moiety. RGB QDs selectively assemble over the printed patterns of P2VP with an adsorption density that depends on the pH of the aqueous dispersions. Besides determination of the maximized adsorption density at pH 5, the unique disintegration of P2VP at low pH values and generation of randomized fluorescence spots within patterned regions have been revealed. This capability has been utilized in the preparation of encoded surfaces with deterministic and stochastic components. A strength of the presented assembly approach is decoupling of the patterning of colloidal nanoparticles from e-jet printing, and thereby facilitating the easy adoption to different materials without need for tedious ink engineering. The presented results establish useful guidelines for future studies on assembly of different colloidal nanomaterials on patterns of P2VP that can be prepared by a portfolio of conventional and unconventional fabrication techniques. Fluorescent carbon dots,[66] for example, are emerging as low-cost and ecofriendly materials for photonics applications.

4. Experimental Section

Chemicals: Silicon wafers (<100>, N/Phos) were purchased from University Wafer Inc. Poly(2-vinylpyridine) (P2VP, Mn = 121.0 kg mol^{-1}, PDI = 1.07) was purchased from Polymer Source Inc. 1,2,4-Trichlorobenzene (anhydrous, ≥99%), zinc acetate (99.99% trace metals basis), cadmium oxide (>99.99% trace metals basis), selenium (pellets, < 5 mm particle size, >99.999% trace metals basis), sulfur (flakes, >99.99% trace metals basis), trioctylphosphine (97%), oleic acid (technical grade, >90%), 1-octadecene (technical grade, 90%), 3-mercaptopropionic acid (>99%), toluene (ACS reagent >99.5%), acetone (ACS reagent >99.5%), hexanes (ReagentPlus >99%), acetonitrile (anhydrous, 99.8%) were purchased from Sigma Aldrich. Hydrochloric acid (1.0 N) and pH indicator sticks (0–14) were purchased from VWR Inc. Sodium Hydroxide was purchased from Wards Science Inc. Deionized (DI) water was purchased from Protocol Inc.

E-Jet Printing: A metal-coated glass capillary nozzle (World Precision Instruments, inner nozzle diameter 1.2 or 5 µm) with a distance of ≈20 µm from the tip to the substrate was placed vertically. The syringe was filled with ≈0.2 mL of 10 wt.% P2VP solution in 1,2,4-trichlorobenzene. The ink was brought to the tip of the syringe needle by applying pressure using a pump. A voltage (250–450 V) bias was applied between the metal-coated

Figure 5. Physically unclonable security labels. a) Schematic illustration of the process. b) AFM images at two magnifications for P2VP features after immobilization of QDs at pH 3. c) Fluorescence microscope images of random arrays of QDs assembled on the P2VP patterns. d) Binary keys derived from the corresponding fluorescence images. e) Proposed fabrication and authentication of the security labels.

syringe needle tip and the grounded substrate to initiate printing. The printing process was performed by using a 5-axis stage interfaced to a computer for coordinated control of the voltage applied to the nozzle.

Synthesis of Metal Complex and Polysulfide Precursors for QDs: 0.5 M Zn-OA Stock Solution: 20 mmol Zn(ac)2, 20 mL OA, and 20 mL 1-ODE were degassed for 1 h at 110 °C, before being heated to 220 °C for 30 min to form a clear solution. The flask can be reheated at 80 °C to liquify the solidified Zn-OA. 0.67 M ODE-S: Briefly, 8 mmol of S powder and 12 mL of ODE were added to a 50 mL RBF and degassed at 110 °C for 30 min, then heated to 180 °C under Ar flow for 30 min to obtain a faint yellow clear solution. The mixture can be reheated to 180 °C if any S precipitates. OA-S 0.8 M: 8 mmol of S powder and 10 mL of OA was added to a 50 mL RBF and degassed at 150 °C for an hour, making a brown solution. The solution was held at 100 °C to avoid crystallization of saturated OA byproducts.

The Synthesis of Red Quantum Dots: 0.2 mmol (25.7 mg) CdO, 3 mmol (549 mg) Zn(ac)2, 3.5 mL oleic acid, and 7.5 mL 1-ODE were loaded into a 50 mL RBF and degassed at 110 °C for 1 h under vacuum before being heated to 300 °C under argon flow and stirring to achieve a clear mixture. Swiftly, 0.25 mL of 0.25M TOP-Se was injected into the flask at 300 °C and the reaction mixture was stirred for 12 min to form a red CdZnSe core. Then, 0.625 mL of 2 M TOP-Se mixed with 1.875 mL of ODE (2.5 mL total volume) was added dropwise at 2 mL h^{-1} (over 75 min) and the reaction mixture was allowed to stir for 20 min to grow the ZnSe shell. Finally, the reactor was cooled to 285 °C with an air jet, where 0.3 mL of 2 M TOP-S mixed with 1.7 mL of ODE was dropwise injected at 8 mL h^{-1} (over 15 min) and allowed to stir at 285 °C for an additional 20 min to form a thin ZnS shell. The reactor was then cooled to room temperature and the product was left in the reaction mixture where it is stable for months.

The Synthesis of Green Quantum Dots: 0.14 mmol CdO, 3.41 mmol Zn(ac)2, 7 mL OA, and 15 mL 1-ODE were loaded into a 100 mL RBF, where it was degassed for 1 h under vacuum, then heated to 310 °C under argon flow and stirred until a clear mixture was achieved. At 310 °C, a 2.1 mL mixture of 1:1 2 M TOP-S and 2 M TOP-Se (1.1 mL each) was swiftly injected and allowed to stir at 310 °C for 10 min to form the CdZnSeS core. 3 mL 0.67 M ODE-S was then injected to the reaction mixture at 12 mL h^{-1} (over 15 min) and allowed to stir at the same temperature for 10 min. Then, 7.5 mL of the 0.5 M Zn-OA stock solution was added at 45 mL h^{-1} (over 10 min) and allowed to stir for 20 min before cooling the reactor to 285 °C. 5 mL of 2 M TOP-S was then added dropwise to the reaction mixture at 15 mL h^{-1} (over 20 min) and allowed to stir for another 20 min to form bright green CdZnSeS/ZnS QDs before cooling to room temperature and the product was left in the reaction mixture, where it is stable for months.

The Synthesis of Blue Quantum Dots: 0.25 mmol (32.1 mg) CdO, 2.5 mmol (457 mg) Zn(ac)2, 1.4 mL OA, 4 mL 1-ODE were loaded in a 50 mL RBF and degassed for 1 h at 110 °C before being heated to 310 °C under Argon flow. At 310 °C, 0.4 mL of the 0.67 M ODE-S stock solution was swiftly injected into the flask and allowed to stir for 12 min to obtain CdZnS QDs. Then, 1.4 mL of 0.8 M OA-S was added dropwise into the flask and stirred for 3 h to form the CdZnS/ZnS QD with deep blue emission. The mixture was then cooled to room temperature and the product was left in the reaction mixture, where it is stable for months.

Transfer of Quantum Dots from Organic to Aqueous Phase: The QDs were phase transferred using a modification of a previously reported method.[67] Briefly, a 1 mL of 0.1 M to 0.125 M 3-MPA solution containing 0.1 mmol NaOH in DI water was prepared. A 1 mL volume of diluted and calibrated solution (OD 0.35, 0.25, 0.35 for RGB QDs in toluene) of QDs in toluene was added to this mixture and stirred overnight. The basic solution drives the equilibrium towards the formation of thiolates which displace surface carboxylates, allowing QDs to be soluble in DI water after precipitation with excess ethanol.

The red QDs were purified as follows. An excess amount of acetone was added to 3 mL of the reaction mixture and the precipitate was collected after centrifugation at 3800 rpm for 5 min. The precipitated QDs were then redissolved into 1 mL of hexanes and any insoluble organics were removed by centrifugation at 3800 rpm for another 5 min. Then, 1 mL of chloroform and 2 mL of acetonitrile was added to the solution, sonicated, and centrifuged at 3800 rpm for 5 min and redissolved into hexanes for phase transfer.

The blue and green QDs were purified in the same manner as the red QDs except for the last purification step where a 2:1 ratio of acetone and ethanol was used instead of chloroform/acetonitrile. This last purification step was also repeated twice more before the final precipitate was redissolved into toluene for phase transfer.

For red QDs, the concentration of QDs was adjusted to obtain an optical density of 0.35 at 380 nm when diluted 30-fold for a 1 cm path length. An equal volume of 1 M NaOH and 0.125 M 3-MPA in DI water was added to the QD solution and stirred overnight. The mixture was then precipitated with excess ethanol and centrifugation at 3800 rpm for 5 min was carried out before the resulting pellet was dried under vacuum and redissolved in 1 mL DI water.

For blue and green QDs, the QDs were diluted to an OD of 0.25 and 0.35 respectively at 400 nm when diluted 30-fold for a 1 cm path length. An equal volume of 1 M NaOH in DI water was then added followed by the addition of 9 µL of 3-MPA and sonicated. Then excess ethanol was swiftly added to the vial and centrifugation at 3800 rpm for 5 min was carried out to yield a compact pellet that can be dissolved in 1 mL of DI water.

pH Adjustment: To each aliquot of as-exchanged QDs, appropriate amount of 0.1 M HCl or 0.1 M NaOH in DI water was added to achieve the desired pH by continuous litmus paper test. Figure S5 in the Supporting Information shows the amount of each acid or base added to a 1 mL solution of QDs in DI water for each color.

Characterization: The morphology of the substrate after printing of the P2VP patterns was analyzed by SEM (Hitachi S-4800) imaging that was performed at 1 kV. The topography of the relevant surfaces was analyzed with AFM (Asylum Research MFP-3D-SA) in tapping mode. All optical microscope images were taken using Olympus MX63L. Fluorescence microscope (Zeiss Stereo Discovery V16 and V20 Microscope) was used to acquire fluorescence images of immobilized QDs. This microscope used a 120 W mercury vapor short arc lamp (X-Cite 120Q) as the light source. TEM was used to analyze morphology of as-synthesized and ligand-exchanged QDs (JEOL 2010FS). UV–vis (Agilent 8453) and PL (HORIBA Jobin Yvon Fluoromax-3) spectroscopy were conducted to ascertain optical features of QDs.

Images Brightness Counting: In ImageJ, to unsaturated fluorescence microscopy images, a low threshold of 5 (noise and dark level out of a total bright value of 255) was applied after grey scaling, rendering maximum brightness values (255/3 = 85). Then, the image counts, and brightness values were multiplied and integrated per the following equation

$$g_{FOM} = \int_{5}^{85} n(x) \times x dx \quad (1)$$

This convolves insight into both the number of immobilized QDs and their corresponding brightness.

PUF Analysis and Feature Matching: A custom program written in MATLAB was used to generate binary keys from the corresponding fluorescence microscope images. An image with a pixel dimension of 144 × 140 was used for the key extraction. A noise reduction and binarization was then performed on these images. Von Neumann debiasing was used for the generation of 256-bits long binary keys. Details of the key extraction process and *p*-values showing the randomness are presented in the supporting information.

Supporting Information

Supporting Information is available from the Wiley Online Library or from the author.

Acknowledgements

This work was supported by the Research Fund of the Erciyes University (Project Number FDK-2021-10759). I.T. acknowledges the financial support from the Scientific and Technological Research Council of

Turkey (TUBITAK) 2211-A National PhD Scholarship Program (app. no: 1649B031901446) and 2214-A International Research Fellowship Programme (app. no: 1059B142000352). I.T. acknowledges the mentorship of Prof. John A. Rogers. M.S. and C.H. gratefully acknowledge financial support from the U.S. National Science Foundation (Grant No. 2132538). The material presented in this work was carried out in part in the Materials Research Laboratory Central Research Facilities, the Micro-Nano-Mechanical Systems Cleanroom Laboratory within the Department of Mechanical Science and Engineering, and the Microscopy Suite in the Beckman Institute for Advanced Science and Technology at the University of Illinois.

Conflict of Interest

The authors declare no conflict of interest.

Data Availability Statement

The data that support the findings of this study are available from the corresponding author upon reasonable request.

Keywords

colloidal quantum dots, encoded surfaces, pH, polymers, printing

Received: July 4, 2023
Revised: August 17, 2023
Published online: September 1, 2023

[1] K.-S. Cho, E. K. Lee, W.-J. Joo, E. Jang, T.-H. Kim, S. J. Lee, S.-J. Kwon, J. Y. Han, B.-K. Kim, B. L. Choi, *Nat. Photonics* **2009**, *3*, 341.
[2] Y. Jiang, S.-Y. Cho, M. Shim, *J. Mater. Chem.* **2018**, *6*, 2618.
[3] D.-Y. Jo, H. Yang, *Chem. Commun.* **2016**, *52*, 709.
[4] H. Liu, M. Li, O. Voznyy, L. Hu, Q. Fu, D. Zhou, Z. Xia, E. H. Sargent, J. Tang, *Adv. Mater.* **2014**, *26*, 2718.
[5] H. Lee, H.-J. Song, M. Shim, C. Lee, *Energy Environ. Sci.* **2020**, *13*, 404.
[6] Y. Wang, K. Wang, X. Hu, Y. k. Wang, W. Gao, Y. Zhang, Z. Liu, Y. Zheng, K. Xu, D. Yang, *ACS Nano* **2023**, *17*, 3696.
[7] J. Guo, H. Li, L. Ling, G. Li, R. Cheng, X. Lu, A.-Q. Xie, Q. Li, C.-F. Wang, S. Chen, *ACS Sustainable Chem. Eng.* **2019**, *8*, 1566.
[8] A. L. Efros, L. E. Brus, *ACS Nano* **2021**, *15*, 6192.
[9] C. Murray, D. J. Norris, M. G. Bawendi, *J. Am. Chem. Soc.* **1993**, *115*, 8706.
[10] Y. Altintas, U. Quliyeva, K. Gungor, O. Erdem, Y. Kelestemur, E. Mutlugun, M. V. Kovalenko, H. V. Demir, *Small* **2019**, *15*, 1804854.
[11] R. C. Page, D. Espinobarro-Velazquez, M. A. Leontiadou, C. Smith, E. A. Lewis, S. J. Haigh, C. Li, H. Radtke, A. Pengpad, F. Bondino, *Small* **2015**, *11*, 1548.
[12] Y. Shu, X. Lin, H. Qin, Z. Hu, Y. Jin, X. Peng, *Angew. Chem.* **2020**, *132*, 22496.
[13] X. Yu, H. Zhang, J. Yu, *Aggregate* **2021**, *2*, 20.
[14] F. Sahin, S. Pekdemir, M. Sakir, Z. Gozutok, M. S. Onses, *Adv. Mater. Interfaces* **2022**, *9*, 2200048.
[15] Y. Liu, F. Han, F. Li, Y. Zhao, M. Chen, Z. Xu, X. Zheng, H. Hu, J. Yao, T. Guo, *Nat. Commun.* **2019**, *10*, 2409.
[16] M. D. Ho, N. Kim, D. Kim, S. M. Cho, H. Chae, *Small* **2014**, *10*, 989.
[17] X. Pi, Q. Li, D. Li, D. Yang, *Sol. Energy Mater. Sol. Cells* **2011**, *95*, 2941.
[18] N. K. Stankovic, M. Bodik, P. Siffalovic, M. Kotlar, M. Micusik, Z. Spitalsky, M. Danko, D. D. Milivojevic, A. Kleinova, P. Kubat, *ACS Sustainable Chem. Eng.* **2018**, *6*, 4154.
[19] T. Shen, J. Yuan, X. Zhong, J. Tian, *J. Mater. Chem.* **2019**, *7*, 6266.
[20] W. Xie, R. Gomes, T. Aubert, S. Bisschop, Y. Zhu, Z. Hens, E. Brainis, D. Van Thourhout, *Nano Lett.* **2015**, *15*, 7481.
[21] S. Wang, X. Dou, L. Chen, Y. Fang, A. Wang, H. Shen, Z. Du, *Nanoscale* **2018**, *10*, 11651.
[22] W. Mei, Z. Zhang, A. Zhang, D. Li, X. Zhang, H. Wang, Z. Chen, Y. Li, X. Li, X. Xu, *Nano Res.* **2020**, *13*, 2485.
[23] J.-S. Park, J. Kyhm, H. H. Kim, S. Jeong, J. Kang, S.-e. Lee, K.-T. Lee, K. Park, N. Barange, J. Han, *Nano Lett.* **2016**, *16*, 6946.
[24] Y. Wang, I. Fedin, H. Zhang, D. V. Talapin, *Science* **2017**, *357*, 385.
[25] D. Hahm, J. Lim, H. Kim, J.-W. Shin, S. Hwang, S. Rhee, J. H. Chang, J. Yang, C. H. Lim, H. Jo, *Nat. Nanotechnol.* **2022**, *17*, 952.
[26] H. Cho, J. A. Pan, H. Wu, X. Lan, I. Coropceanu, Y. Wang, W. Cho, E. A. Hill, J. S. Anderson, D. V. Talapin, *Adv. Mater.* **2020**, *32*, 2003805.
[27] H. Cho, J. Kwak, J. Lim, M. Park, D. Lee, W. K. Bae, Y. S. Kim, K. Char, S. Lee, C. Lee, *ACS Appl. Mater. Interfaces* **2015**, *7*, 10828.
[28] H. Keum, Y. Jiang, J. K. Park, J. C. Flanagan, M. Shim, S. Kim, *ACS Nano* **2018**, *12*, 10024.
[29] M. K. Choi, J. Yang, K. Kang, D. C. Kim, C. Choi, C. Park, S. J. Kim, S. I. Chae, T.-H. Kim, J. H. Kim, *Nat. Commun.* **2015**, *6*, 7149.
[30] T.-H. Kim, K.-S. Cho, E. K. Lee, S. J. Lee, J. Chae, J. W. Kim, D. H. Kim, J.-Y. Kwon, G. Amaratunga, S. Y. Lee, *Nat Photonics* **2011**, *5*, 176.
[31] B. Bao, M. Li, Y. Li, J. Jiang, Z. Gu, X. Zhang, L. Jiang, Y. Song, *Small* **2015**, *11*, 1649.
[32] P. Yang, L. Zhang, D. J. Kang, R. Strahl, T. Kraus, *Adv. Opt. Mater.* **2020**, *8*, 1901429.
[33] B. H. Kim, M. S. Onses, J. B. Lim, S. Nam, N. Oh, H. Kim, K. J. Yu, J. W. Lee, J.-H. Kim, S.-K. Kang, *Nano Lett.* **2015**, *15*, 969.
[34] B. Bangalore Rajeeva, L. Lin, E. P. Perillo, X. Peng, W. W. Yu, A. K. Dunn, Y. Zheng, *ACS Appl Mater Interfaces* **2017**, *9*, 16725.
[35] F. Dawood, J. Wang, P. A. Schulze, C. J. Sheehan, M. R. Buck, A. M. Dennis, S. Majumder, S. Krishnamurthy, M. Ticknor, I. Staude, *Small* **2018**, *14*, 1801503.
[36] M. S. Onses, E. Sutanto, P. M. Ferreira, A. G. Alleyne, J. A. Rogers, *Small* **2015**, *11*, 4237.
[37] S. Malynych, I. Luzinov, G. Chumanov, *J. Phys. Chem. B* **2002**, *106*, 1280.
[38] I. Tokareva, S. Minko, J. H. Fendler, E. Hutter, *J. Am. Chem. Soc.* **2004**, *126*, 15950.
[39] N. Torun, I. Torun, M. Sakir, M. Kalay, M. S. Onses, *ACS Appl. Mater. Interfaces* **2021**, *13*, 11247.
[40] D. Nepal, M. S. Onses, K. Park, M. Jespersen, C. J. Thode, P. F. Nealey, R. A. Vaia, *ACS Nano* **2012**, *6*, 5693.
[41] N. B. Kiremitler, I. Torun, Y. Altintas, J. Patarroyo, H. V. Demir, V. F. Puntes, E. Mutlugun, M. S. Onses, *Nanoscale* **2020**, *12*, 895.
[42] S. Pekdemir, I. Torun, M. Sakir, M. Ruzi, J. A. Rogers, M. S. Onses, *ACS Nano* **2020**, *14*, 8276.
[43] Y. Altintas, I. Torun, A. F. Yazici, E. Beskazak, T. Erdem, M. S. Onses, E. Mutlugun, *Chem. Eng. J.* **2020**, *380*, 122493.
[44] S. F. Wuister, I. Swart, F. van Driel, S. G. Hickey, C. de Mello Donega, *Nano Lett.* **2003**, *3*, 503.
[45] M. S. Onses, A. Ramírez-Hernández, S.-M. Hur, E. Sutanto, L. Williamson, A. G. Alleyne, P. F. Nealey, J. J. De Pablo, J. A. Rogers, *ACS Nano* **2014**, *8*, 6606.
[46] M. S. Onses, C. Song, L. Williamson, E. Sutanto, P. M. Ferreira, A. G. Alleyne, P. F. Nealey, H. Ahn, J. A. Rogers, *Nat. Nanotechnol.* **2013**, *8*, 667.
[47] P. J. Yunker, T. Still, M. A. Lohr, A. Yodh, *Nature* **2011**, *476*, 308.
[48] X. Jin, K. Xie, T. Zhang, H. Lian, Z. Zhang, B. Xu, D. Li, Q. Li, *Chem. Commun.* **2020**, *56*, 6130.
[49] B. Xu, T. Zhang, X. Lin, H. Yang, X. Jin, Z. Huang, Z. Zhang, D. Li, Q. Li, *Opt. Mater. Express* **2020**, *10*, 1232.
[50] R. Singh, S. Akhil, V. V. Dutt, N. Mishra, *Nanoscale Adv.* **2021**, *3*, 6984.
[51] J. Zheng, F. Gao, G. Wei, W. Yang, *Chem. Phys. Lett.* **2012**, *519*, 73.
[52] J. G. Kennemur, *Macromol. Chem. (Oxford)* **2019**, *52*, 1354.

[53] Y. Roiter, S. Minko, *J. Am. Chem. Soc.* **2005**, *127*, 15688.
[54] S. Singamaneni, M. E. McConney, V. V. Tsukruk, *Adv. Mater.* **2010**, *22*, 1263.
[55] S. Singamaneni, M. E. McConney, V. V. Tsukruk, *ACS Nano* **2010**, *4*, 2327.
[56] H. Yilmaz, S. Pekdemir, H. H. Ipekci, N. B. Kiremitler, M. Hancer, M. S. Onses, *Appl. Surf. Sci.* **2016**, *385*, 299.
[57] N. Kayaci, R. Ozdemir, M. Kalay, N. B. Kiremitler, H. Usta, M. S. Onses, *Adv. Funct. Mater.* **2022**, *32*, 2108675.
[58] S. Yakunin, J. Chaaban, B. M. Benin, I. Cherniukh, C. Bernasconi, A. Landuyt, Y. Shynkarenko, S. Bolat, C. Hofer, Y. E. Romanyuk, *Nat. Commun.* **2021**, *12*, 981.
[59] L. Zhu, D. Shen, Q. Wang, K. H. Luo, *ACS Appl. Mater. Interfaces* **2021**, *13*, 56465.
[60] R. Pappu, B. Recht, J. Taylor, N. Gershenfeld, *Science* **2002**, *297*, 2026.
[61] T. McGrath, I. E. Bagci, Z. M. Wang, U. Roedig, R. J. Young, *Appl. Phys. Rev.* **2019**, *6*, 011303.
[62] L. Tian, K.-K. Liu, M. Fei, S. Tadepalli, S. Cao, J. A. Geldmeier, V. V. Tsukruk, S. Singamaneni, *ACS Appl. Mater. Interfaces* **2016**, *8*, 4031.
[63] R. Arppe, T. J. Sørensen, *Nat. Rev. Chem.* **2017**, *1*, 0031.
[64] E. Rublee, V. Rabaud, K. Konolige, G. Bradski, presented at *2011 International Conference on Computer Vision* **2011**.
[65] A. Esidir, N. B. Kiremitler, M. Kalay, A. Basturk, M. S. Onses, *ACS Appl. Polym. Mater.* **2022**, *4*, 5952.
[66] J. Li, X. Gong, *Small* **2022**, *18*, 2205099.
[67] A. Lesiak, M. Banski, K. Halicka, J. Cabaj, A. Żak, A. Podhorodecki, *Nanotechnology* **2020**, *32*, 075705.